

On integrating Monte Carlo calculations in and around near-critical configurations – II. Pressurized water reactors

M. Brovchenko^a, K.W. Burn^{b,*}, P. Console Camprini^c

^a IRSN (Institut de Radioprotection et de Sécurité Nucléaire), 31 avenue de la Division Leclerc 92260 Fontenay aux Roses CEDEX, France

^b ENEA (National Agency for New Technology, Energy and Sustainable Economic Development) (retired), Via M.M.Sole, 4, 40129 Bologna, Italy

^c ENEA (National Agency for New Technology, Energy and Sustainable Economic Development), Via M.M.Sole, 4, 40129 Bologna, Italy

ARTICLE INFO

This paper is dedicated to the memory of Arie Dubi (1944–2015), the originator of the DSA and a pioneering Monte Carlo developer

Keywords:

Monte Carlo
Variance reduction
Direct Statistical Approach
Decoupled approach
Eigenvalue calculation
Reactor core

ABSTRACT

This article is the second part of a paper that evaluates a recent approach that has been developed to calculate differential in- and ex-fissile configuration responses employing Monte Carlo with variance reduction. The first part focused more on the methodological aspects and established the circumstances under which a single eigenvalue calculation could be made as efficient as possible, in particular as compared with an empirical approach (involving again a single eigenvalue calculation). Both ex- and in-core test problems were considered. Instead this second part looks at two ex-core PWR sample problems and compares the single eigenvalue approach with an all Monte Carlo decoupled approach with different approximations at the point of decoupling, thus highlighting the sensitivity of the decoupled result to the decoupling approximation

1. Introduction

In the last few years an innovative Monte Carlo approach for calculating localized radiation responses in and around critical configurations under conditions of relatively high attenuation has been developed (Brovchenko et al., 2022; Console Camprini et al., 2021). It is based on the DSA (“Direct Statistical Approach” to optimizing population/weight control in Monte Carlo (Burn, 2014a; Burn, 2015)). We name it “the single eigenvalue approach”. In part I we restricted ourselves to analyzing the new approach. We compared it with an empirical approach involving analog (i.e. no) variance reduction (VR) in the fissile zone and VR outside. We saw under what circumstances the new approach is more efficient than the empirical approach, and by how much. We also saw how we can improve the new approach.

In this work, employing two ex-core problems we compare the new approach to various decoupling approximations. The problems involve the radiation damage to the pressure vessel (PV) and the ex-core neutron detector signal in the PV well of two PWR models, GEN II and GEN III. In the PWR GEN III model (which is the same geometric model as in part I (Brovchenko et al., 2022; Console Camprini et al., 2021) but with a slightly different core composition), we also consider activation

responses in the concrete shielding outside the PV well.

The new approach was introduced in (Burn, 2014; Burn, 2015; Burn, 2014). MCNP6 ver. 1.0 (Goorley et al., 2013) is employed as a vehicle, with the new methodology written as modifications in “patch” form. Three features are highlighted in (Brovchenko et al., 2022; Console Camprini et al., 2021):

- As well as playing an important role in maintaining the stability of the fundamental mode (Burn and Console Camprini, 2017), super-histories (Brissenden and Garlick, 1986) help to reduce the variance. Their various roles are summarized in (Burn and Console Camprini, 2018).
- A multi-response optimization is carried out with all the responses-of-interest which are named the “local responses” together with a sufficient number of fission source tallies to mock up the fundamental mode. The latter are named the “global responses”.
- “Fictitious source” cells are introduced to improve the sampling of the fission source and thus help to reduce the variance.

For in-core problems the new approach aims to provide results of a higher quality compared with analog or alternatively to allow to

* Corresponding author.

E-mail addresses: mariya.brovchenko@irsn.fr (M. Brovchenko), kennethwilliamburn@gmail.com (K.W. Burn), patrizio.consolecamprini@enea.it (P.C. Camprini).

<https://doi.org/10.1016/j.anucene.2022.109417>

Received 2 April 2022; Received in revised form 1 August 2022; Accepted 23 August 2022

Available online 29 September 2022

0306-4549/© 2022 Elsevier Ltd. All rights reserved.

calculate responses previously considered unfeasible. For ex-core problems, decoupling is avoided with the ex-core responses calculated within the eigenvalue calculation.

Here we do not look to optimize the new approach in the way that was done in part I (for example we do not employ fictitious source cells and do not consider the figure-of-merits (FOM's) (Brovchenko et al., 2022; Console Camprini et al., 2021). Rather we use the new approach to evaluate various approximations in a decoupled approach. The decoupled approach that we adopted employed the fission sites as the point of decoupling (Console Camprini et al., 2022).

MCNP (Goorley et al., 2013) already allows fission sites to be written to file WSSA in an eigenvalue calculation. These sites are subsequently read from the same file RSSA (=WSSA) in a fixed source calculation (with fissions treated as absorptions) in which VR is employed and the tallies are made. Although this is probably currently the most common method of decoupling, at least if using MCNP, we instead employed an older approach described as follows:

As the angular distribution of the fission neutrons is isotropic in the lab. system, the approximations at the point of decoupling only concern the energy and spatial distributions. The spatial variable is binned whilst various analytic functions are used to describe the fission neutron energy. We name this decoupling approach: “spatial binning / analytic energy”. (A possible alternative approach, to use the core leakage current, binning the space, energy and angular variables, was rejected due to the added requirement to bin the angular and energy variables.)

For the energy, we employ one of three fixed analytical Watt fission spectra:

$$p(E) = C \cdot \exp(-E/a) \cdot \sinh(\sqrt{bE})$$

that require to define two parameters, a (MeV) and b (MeV^{-1}) for thermal neutron-induced fission either in ^{235}U ($a = 0.988$; $b = 2.249$) or in ^{239}Pu ($a = 0.966$; $b = 2.842$), or a default spectrum available in MCNP ($a = 0.965$; $b = 2.29$) (Goorley et al., 2013). (Instead in (Vuiart et al., 2021) a more sophisticated approach to the energy distribution of the fission neutrons in the decoupled approach is examined.)

Various ways of executing the spatial binning are considered, some of which require patching MCNP (thereby introducing QA issues). Comparison of the results employing these spatial binning options and the three energy spectra with the single eigenvalue approach results, forms the principal basis of this paper.

The reasons for the adoption of this particular approach to decoupling are discussed in the following where we list the advantages and disadvantages of the two decoupling approaches:

- The WSS/RSS approach makes no approximations at the point of decoupling. It also correctly calculates the statistical errors on the tallies in the second (fixed source) calculation. However the statistical errors may be limited by the size of the first (eigenvalue) calculation and the number of fission neutrons run in the eigenvalue calculation is limited by the allowable size of the WSSA file. (In the problems in §2 and §3 a total of 5×10^8 and 1.2×10^8 fission neutrons respectively were run in the active cycles of the eigenvalue calculation, which might prove challenging when writing fission source points to file.)
- The older approach of spatial binning with analytic energy distribution has multiple disadvantages: approximations in space and energy at the point of decoupling (which will be examined in this paper); statistical errors on the tallies that only derive from the second (fixed source) calculation; for some (finer) spatial approximations, the necessity of patching MCNP, thus reducing the QA. The advantage is that the size of the eigenvalue calculation is only limited by the computing time.

In some problems the precise spatial location and energy of the fission neutrons may not be of critical importance. In this case the spatial

binning / analytic energy approach with a one-off eigenvalue calculation, even if time-consuming, may be advantageous. Instead in other problems, the precise spatial location and energy can be very important, and for these problems the spatial binning / analytic energy approach may give poorer results than the WSS/RSS approach.

The question of the statistical uncertainty on the tallies and “up-stream” on the distribution of fissions, deserves a little further discussion. The edges (top, bottom, side) of the core provide the major contributions to ex-core responses. The first eigenvalue calculation must adequately sample such regions. Indeed with serious undersampling, there may occur the usual danger in Monte Carlo simulations of tally results with a small statistical uncertainty being wrong as the actual problem is not being sampled. This may not be evident employing the WSS/RSS approach (and indeed employing the single eigenvalue approach to which it bears some resemblance). Instead the spatial binning / analytic energy approach does allow to analyze the fission distribution and identify any inadequately sampled regions.

2. PWR GEN II

The PWR GEN II model has a conventional arrangement of a water reflector between the baffle and the barrel and neutron pads in the inner part of the downcomer to protect the PV. A vertical section of the GEN II reactor model is shown in Fig. 1. The PV damage was evaluated at the core mid-plane at a number of azimuthal positions shown in the horizontal section in Fig. 2. The positions at which the damage was evaluated each subtended an azimuthal angle of 2° and had a height of 20 cm. Gamma transport was not made and the responses of interest were the total neutron fluxes with energy above 1 MeV and above 100 keV respectively on the PV. Fig. 2 also shows the positions of the ex-core detectors at 45° and 225° . A vertical section through the ex-core detectors is shown in Fig. 3. Fig. 4 shows a detail of the ex-core detector at 45° . A thin amorphous film of ^{10}B was assumed to cover the inner surface over the central $\frac{1}{2}$ height of the detector. The response-of-interest was the $^{10}\text{B}(n,\alpha)$ rate in the film averaged over both detectors.

Starting from a mixed UOX/MOX core at equilibrium cycle, end-of-cycle assembly-wise fuel compositions were employed with no axial variation. The $^{239}\text{Pu} / (^{239}\text{Pu} + ^{235}\text{U})$ (at.) ratio had a range that varied according to the type of assembly: for the UOX assemblies this range was 0.092 – 0.51 whilst for the MOX assemblies it was 0.90 – 0.96. Fig. 5 shows the assembly configuration at BOL with the two kinds of assembly. We see that the two kinds of assembly are distributed reasonably evenly in the core and in the outer assembly ring.

The neutron cross-section data were based where possible on ENDF/B-VII.1 (Conlin et al., 2013), as were the thermal neutron $S(\alpha,\beta)$ data

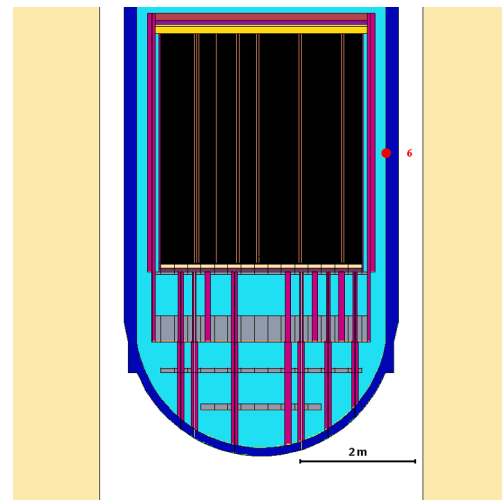


Fig. 1. PWR GEN II: Vertical section.

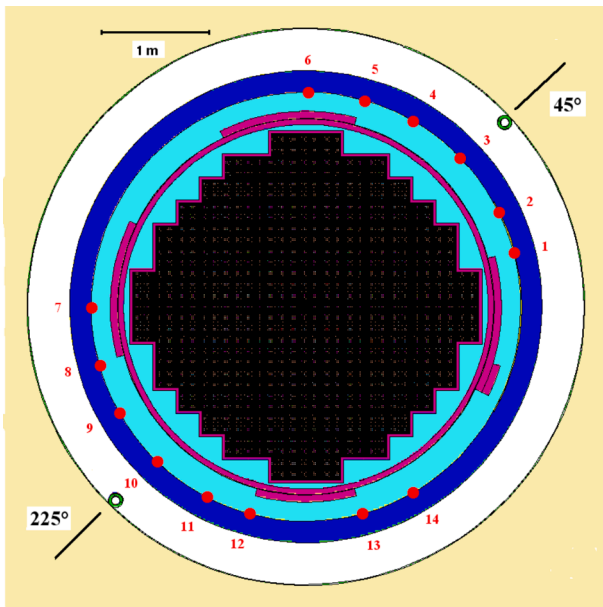


Fig. 2. PWR GEN II: Horizontal section at the core mid-plane.

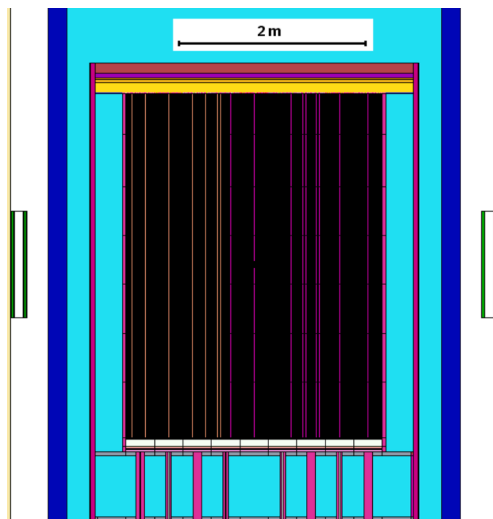


Fig. 3. PWR GEN II: Vertical section with ex-core detectors.

(Conlin and Parsons, 2014) (hydrogen in light water and hydrogen in polyethylene in the ex-core neutron detector).

2.1. Methodology

The single eigenvalue calculation required by the new approach employed a superhistory of 10 fission generations without fictitious source cells (Brovchenko et al., 2022; Console Camprini et al., 2021). To model the global responses, the fissile zone was divided into 12 segments (with 3 radial and 7 axial divisions but actually unifying the axial segments above and below the middle one making thus 4 symmetric axial segments). The 12 fissile zone segments were identical to those that were subsequently employed for the VR. Further details of the methodology may be found in (Brovchenko et al., 2022; Console Camprini et al., 2021; Console Camprini et al., 2022).

For the decoupled calculations, the point of decoupling was the fission sites. The axial binning of the fission sites employed 32 bins with a structure shown in Fig. 5 in (Console Camprini et al., 2022). Radial binning was pin-wise. Each pin was divided into two radial segments of

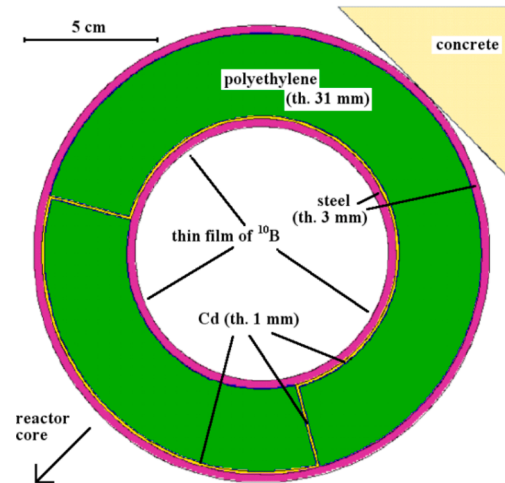


Fig. 4. PWR GEN II: ex-core detector horizontal section.

equal area, with each segment having its own axial distribution. This is referred to as the “dual pin-wise description” of the fission sites. Only for the case of the ex-core neutron detector, an assembly-wise radial binning was also modelled, with each assembly having its own axial distribution. This is referred to as the “assembly-wise description” of the fission sites.

The first part of the decoupled calculation was an eigenvalue calculation with no VR. Having reached the fundamental mode, 10^6 neutrons per fission generation and 500 fission generations were run. The fission sites in the appropriate spatial binning were written to a MCTAL file (Goorley et al., 2013). The statistical error in this calculation, although small, did not appear in the final error estimates.

The energy of the neutrons in the second part of the decoupled calculation was chosen from three possible analytic functions: all three Watt fission spectra with parameters corresponding to the MCNP default, fission of ^{235}U and of ^{239}Pu , the latter two induced by thermal neutrons (Goorley et al., 2013). Note that MCNP required patching to accept the pin-wise source. This involved modifying the *source* subroutine and recompiling.

The VR for the second part of the decoupled calculation was taken from the eigenvalue case with parameters generated by the DSA then converted to a weight window (Goorley et al., 2013).

Finally three calculations were made with the three energy spectra each with a homogeneous spatial distribution of the fission sites in the core (homogeneous throughout the core including cladding and coolant, delimited by the outer surfaces of the assemblies). These cases did not of course require a preliminary eigenvalue calculation to tally the fission source. The results of these calculations are given in (Console Camprini et al., 2022).

2.2. Results

Results of the single eigenvalue Monte Carlo calculations, normalized to 1 W of thermal power are given in (Console Camprini et al., 2022). Instead here we are primarily interested in the comparison between the single eigenvalue results and the decoupled results.

Figs. 6–8 show the ratio: decoupled result to eigenvalue result, for the three source spectra: default, ^{235}U and ^{239}Pu respectively. Two standard deviation error bars are present in all the figures but they may be concealed by the data points. The errors in these figures take into account both the statistical error in the eigenvalue calculation and that in the second part of the decoupled calculation, but not the statistical error in the first part of the decoupled calculation.

From Figs. 6 to 8:

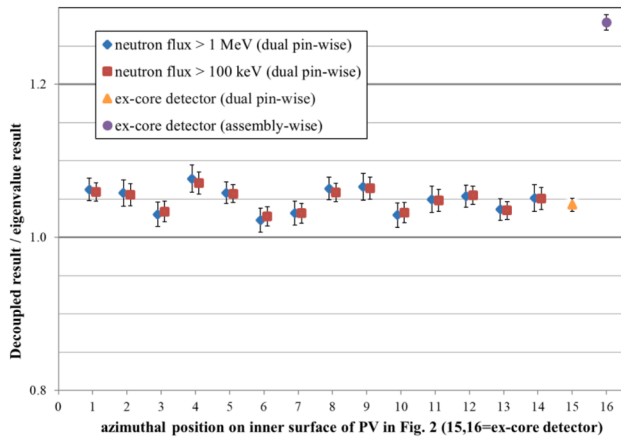


Fig. 8. PWR GEN II: Ratio of decoupled to eigenvalue result for the Watt spectrum for thermal neutron-induced fission in ²³⁹Pu for the dual pin-wise description of fission sites (plus the assembly-wise description for the ex-core detectors).

An important characteristic of the GEN III PWR model is a radial steel reflector just outside the core. While lowering the PV damage compared with the normal water reflector of §2, it increases the neutron reflection back into the fissile region and thereby increases the importance of higher eigenmodes (Sargeni et al., 2014). As a result, a Monte Carlo simulation has a greater difficulty to reach and maintain the fundamental mode (Burn and Console Camprini, 2017).

A vertical section of the GEN III reactor model is shown in Fig. 9. Figs. 10 and 11 show horizontal sections at the core mid-plane. Figs. 12 and 13 show horizontal sections at and just below the platforms respectively.

There were three sets of radiation responses. The first set measured damage at the internal surface of the PV and included both neutron and γ responses (the γ part just to test the methodology). The second was an ex-core neutron detector in the PV well similar to that in §2. The third set consisted of a number of activation rates of isotopes commonly found in concrete and rebar, at two depths in the concrete shielding surrounding the PV well. We also included in this set the neutron dose (Veinot and Hertel, 2005).

The two principal gauges of the vessel damage are the neutron fluxes with energy >1 MeV and >100 keV. Here mainly for methodological verification, we also employed dpa (displacements per atom), both neutron-induced (Konobeyev and Voukelatou, 2005) and γ -induced (for Fe only, Table 3 in (Blakeman, 2000) – note that the threshold is 700 keV). The three vertical positions where the PV damage is evaluated

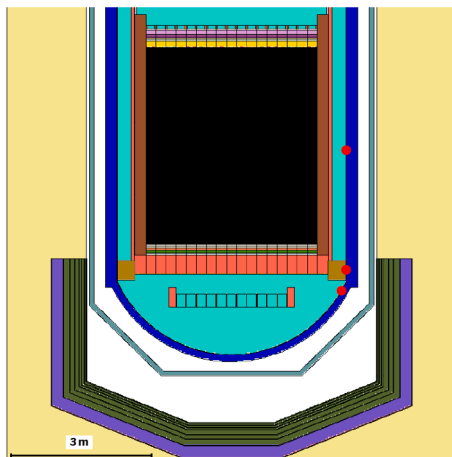


Fig. 9. PWR GEN III: Vertical section.

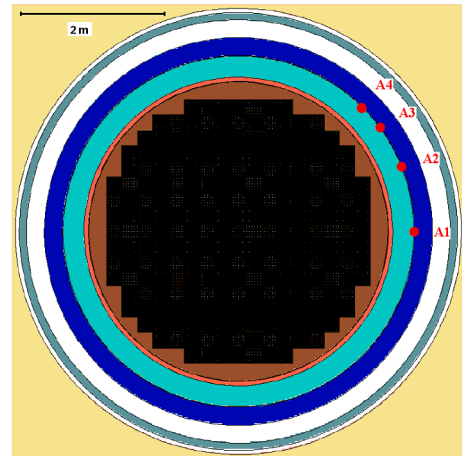


Fig. 10. PWR GEN III: Horizontal section at core mid-plane.

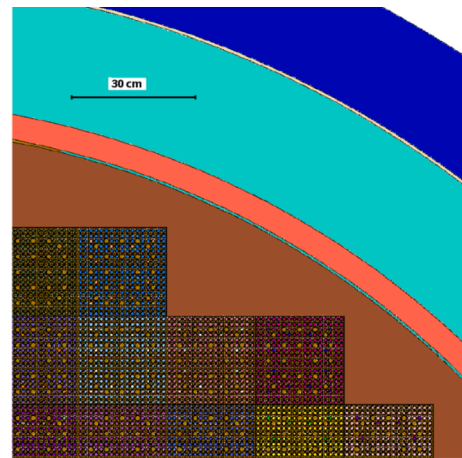


Fig. 11. PWR GEN III: Horizontal section (detail).

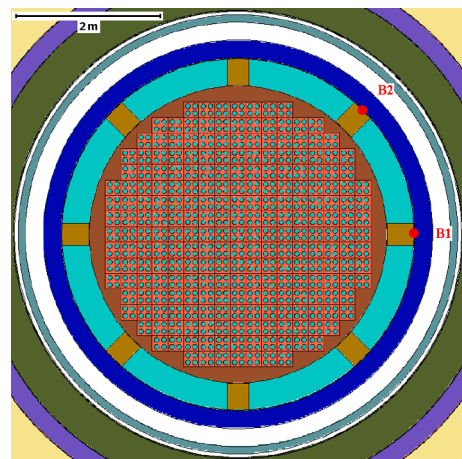


Fig. 12. PWR GEN III: Horizontal section at the supporting platforms.

are shown in Fig. 9 as red dots (at the core mid-plane, at the supporting platforms and just below the platforms where the PV thickness is reduced).

At the core mid-plane and just below the platforms there are four azimuthal positions (A1 – A4 in Fig. 10, C1 – C4 in Fig. 13), and two positions at the platforms (B1 and B2 in Fig. 12). Thus there were 4 requested results at each of 10 positions making 40 responses. Each

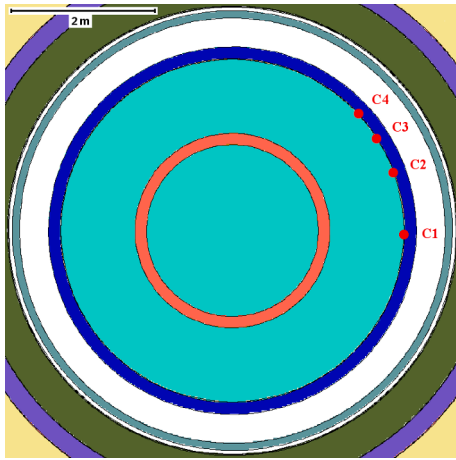


Fig. 13. PWR GEN III: Horizontal section just below the supporting platforms.

position at the mid-plane and below the platform subtends an azimuthal angle of 2° and has a height of 20 cm. The two positions at the platform are slightly larger.

The ex-core neutron detector was similar to the one employed in the PWR GEN II model (Fig. 4). Its location is shown in Figs. 14 and 15. We took the average signal from the 4 detectors. As for PWR GEN II we assumed that the sensitive part of the detector occupied the central axial part over $\frac{1}{2}$ the physical length.

At depths of 15 cm and 150 cm in the radial concrete shielding (Fig. 16), we considered the following activation rates: $^{59}\text{Co}(n,\gamma)$, $^{151}\text{Eu}(n,\gamma)$, $^{153}\text{Eu}(n,\gamma)$, $^{54}\text{Fe}(n,\gamma)$ and $^{56}\text{Fe}(n,2n)$. Note that the $(n,2n)$ reaction has a threshold at around 11.5 MeV. The Fe was in rebar assumed 3% by vol. mixed homogeneously in the concrete, while the Co, an impurity of the Fe, was assumed 100 ppm by weight in the rebar. (Homogeneously mixing the rebar in the concrete neglects self-shielding effects and may result in overestimates of the $^{56}\text{Fe}(n,2n)$ and $^{59}\text{Co}(n,\gamma)$ rates. However, we are primarily interested here in reaction rate ratios and we expect these to be much less sensitive to such approximations in the geometrical model.) The Eu was assumed 4 ppm by weight in the concrete. We tallied these responses over a height equal to that of the fissile zone and on 360° .

Starting from a UOX core at equilibrium cycle, end-of-cycle assembly-wise fuel compositions were employed with no axial variation. The $^{239}\text{Pu} / (^{239}\text{Pu} + ^{235}\text{U})$ (at.) ratio had a range that varied from 0.13 to 0.68, with a reasonably even distribution of the assemblies in the core and in the outer assembly ring. The outer assembly ring is the most important part of the core for most of the ex-core responses considered,

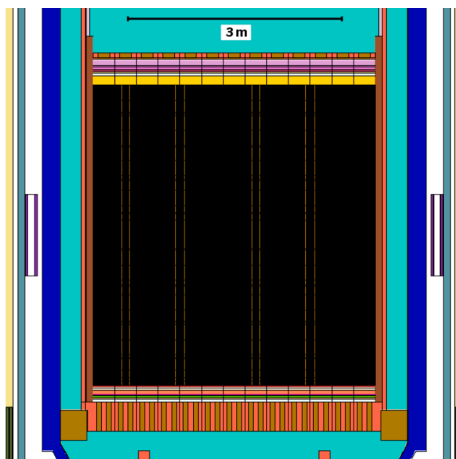


Fig. 14. PWR GEN III: Vertical section showing ex-core detectors.

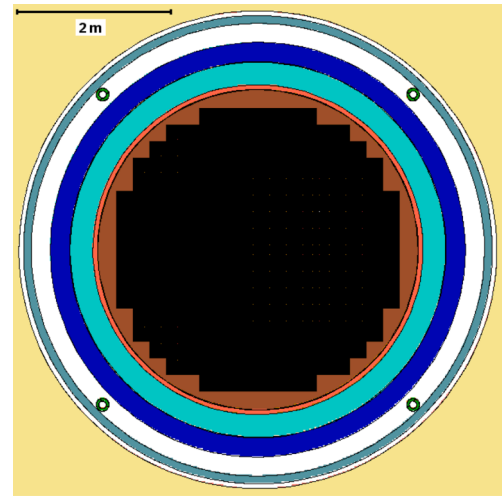


Fig. 15. PWR GEN III: Horizontal section showing ex-core detectors.

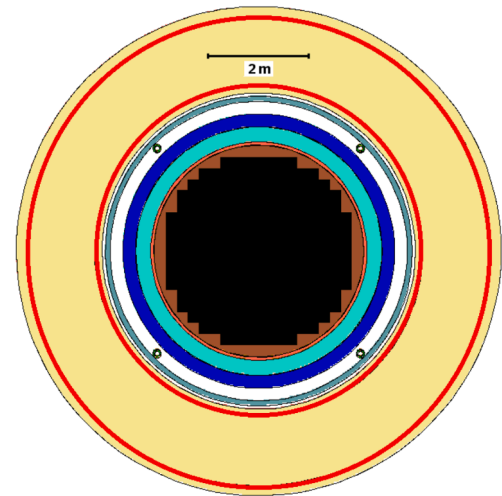


Fig. 16. PWR GEN III: Horizontal section showing location of concrete activation surfaces.

and its average $^{239}\text{Pu} / (^{239}\text{Pu} + ^{235}\text{U})$ ratio is around 0.30.

As for the PWR GEN II model, the neutron cross-section data were based, where possible, on ENDF/B-VII.1 (Conlin et al., 2013). The only difference was that thermal neutron $S(\alpha; \beta)$ data for hydrogen in light water were based on ENDF/B-VII Release 0 (Trellue and Little, 2008) (rather than Release 1 for PWR GEN II (Conlin and Parsons, 2014).

3.1. Methodology

The methodology closely followed that of the GEN II model in §2.1. The single eigenvalue calculation of the new approach employed a superhistory of 10 fission generations without fictitious source cells. To model the global responses, the fissile zone was divided into 12 segments (3 radial and 4 axial) and the 40 ex-core responses were mocked up by 24 local responses (just to generate the VR parameters). The 12 fissile zone segments were identical to those that were subsequently employed for the VR. Further discussion of the methodology may be found in (Brovchenko et al., 2022; Console Camprini et al., 2021; Console Camprini et al., 2022).

The series of decoupled calculations employed the fission sites as the point of decoupling and required patching MCNP. The first part of the decoupled calculation was an eigenvalue calculation with no VR. Having

reached the fundamental mode, 10^6 neutrons per fission generation and 120 fission generations were run. The fission sites in the appropriate spatial binning were written to a MCTAL file (Goorley et al., 2013).

For the radial distribution of fission sites, a more extensive analysis was made compared with PWR GEN II. Both assembly-wise and pin-wise distributions were tested. The assembly-wise distribution mode used two axial distribution options: a single average axial distribution for all the assemblies and each assembly having its own axial distribution. The former is referred to as the “mono-axial assembly-wise description” and the latter as the “assembly-wise description” as for PWR GEN II. The pin-wise distribution mode had each pin with its own axial distribution but with two options: radially homogeneous over each pin or radially homogeneous in each of two radial bins (of equal area) in each pin (with each radial bin having its own axial distribution). The former is referred to as the “pin-wise description” and the latter as the “dual pin-wise description” as for PWR GEN II. A single axial binning was employed consisting of 52 axial bins with a distribution shown in Fig. 17 (with a detail of the lower 15 bins). The final case was a homogeneous fission source throughout the fissile volume (including cladding and water).

The energy at the point of decoupling was treated in the same way as for PWR GEN II with three possible Watt analytic fission spectra: MCNP default, ^{235}U and ^{239}Pu (Goorley et al., 2013).

The responses in the first set (PV damage) were evaluated with all the spatial decoupling approximations. The ex-core detector signal was only treated with the dual pin-wise description and the homogeneous approximation. The responses in the third set were evaluated with the dual pin-wise description, the assembly-wise description (excluding the neutron dose) and the homogeneous approximation (again excluding the neutron dose).

As in the PWR GEN II analysis, the VR parameters, generated in the single eigenvalue calculation of the new approach, were then employed in the second part of the decoupled calculation.

3.2. Results

In (Console Camprini et al., 2022) for reference are shown the absolute results obtained with the eigenvalue calculation. Also in (Console Camprini et al., 2022) are given the results of the homogeneous case and with the mono-axial assembly-wise description, with the decoupled results presented as ratios relative to the eigenvalue results. In the same way in the following sections the decoupled results are presented as ratios relative to the eigenvalue results. §3.2.1 contains the assembly-wise results and §3.2.2 the pin-wise results. Then in §3.2.3 for selected responses we look at the variation of response with energy spectrum and

with the spatial description of the fission sites. (The same variations for the responses other than those selected in §3.2.3 are given in §3.2.4 of (Console Camprini et al., 2022).) Two standard deviation error bars are present in all the figures but may be concealed by the data points.

3.2.1. Assembly-wise fission source results

The assembly-wise description was employed for the PV damage responses and for the reaction rates in the concrete but not for the neutron dose in the concrete nor for the ex-core neutron detector. Figs. 18–20 show the ratios: decoupled / eigenvalue result at the core mid-plane and in the concrete for the Watt fission spectrum with parameters: MCNP default, neutron-induced fission in ^{235}U and in ^{239}Pu respectively.

In Figs. 18–20 we see an overestimation of the decoupled approach for all the PV damage responses for all three spectra. We also see an overestimation of the decoupled approach for the (n,γ) responses at 15 cm depth in the concrete again for all three spectra. Comparing Figs. 18 – 20 to Figs. 19 – 21 in (Console Camprini et al., 2022) for the homogeneous case results we see that this assembly-wise approximation is superior to the homogeneous approximation with the exception of the (n,2n) reaction. This is due in the homogeneous case to cancellation of errors: the spatial approximation overestimates the result and the energy

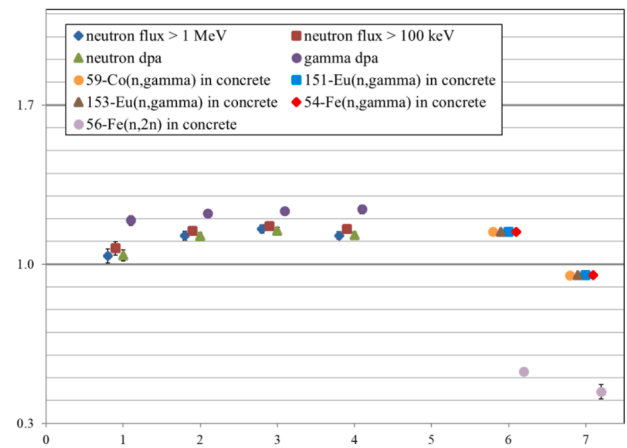


Fig. 18. PWR GEN III: Ratio of decoupled to eigenvalue result for the MCNP default Watt fission spectrum and the assembly-wise description of fission sites (x: 1– 4: A1–A4 in Fig. 10; 6, 7: concrete shielding at 15, 150 cm depth).

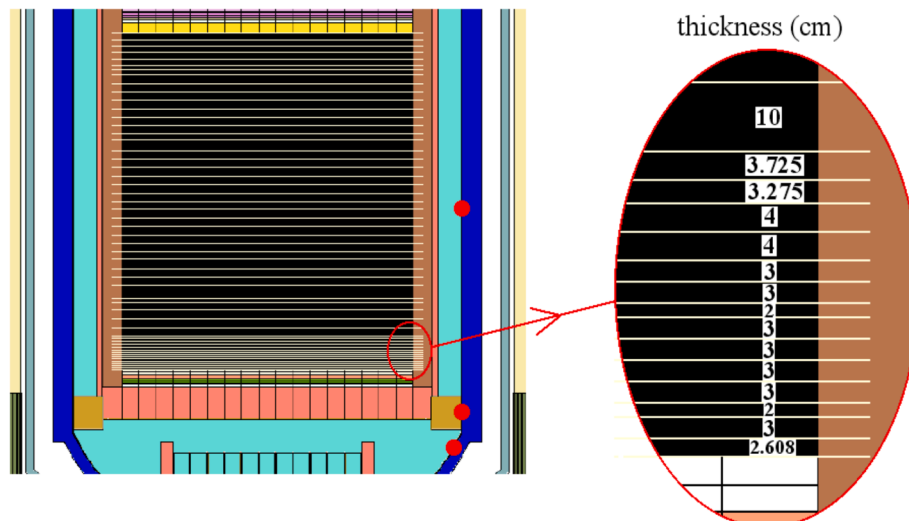


Fig. 17. PWR GEN III: Axial division of fissile zone for decoupling.

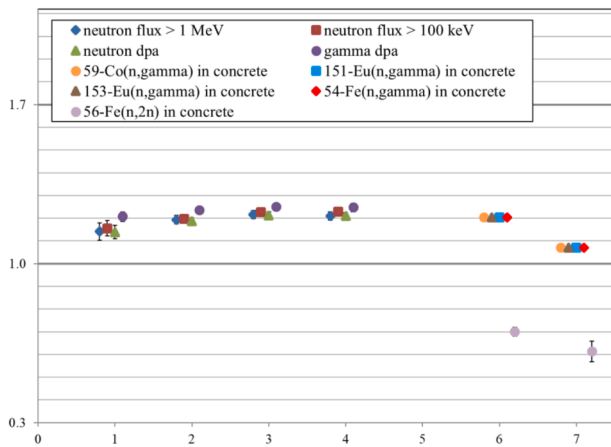


Fig. 19. PWR GEN III: Ratio of decoupled to eigenvalue result for the Watt spectrum for thermal neutron-induced fission in ^{235}U and the assembly-wise description of fission sites (x: 1– 4: A1–A4 in Fig. 10; 6, 7: concrete shielding at 15, 150 cm depth).

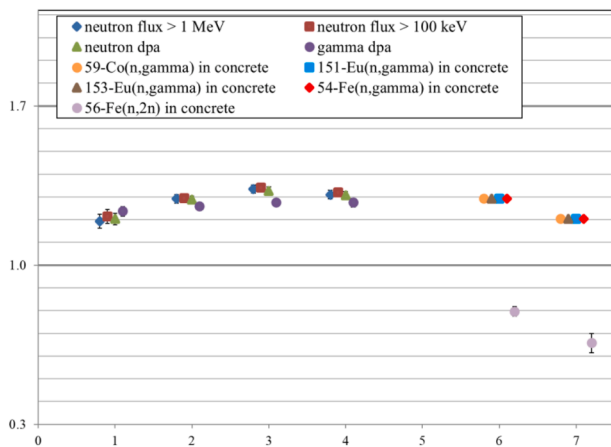


Fig. 20. PWR GEN III: Ratio of decoupled to eigenvalue result for the Watt spectrum for thermal neutron-induced fission in ^{239}Pu and the assembly-wise description of fission sites (x: 1– 4: A1–A4 in Fig. 10; 6, 7: concrete shielding at 15, 150 cm depth).

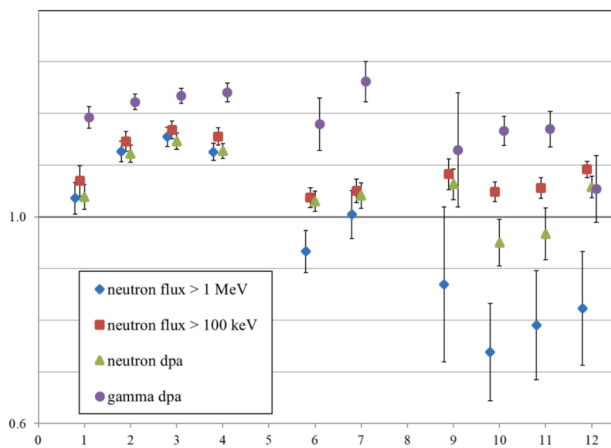


Fig. 21. PWR GEN III: Ratio of decoupled to eigenvalue result for the MCNP default Watt fission spectrum and the assembly-wise description of fission sites (x: 1–4: A1–A4 in Fig. 10; 6, 7: B1, B2 in Fig. 12; 9–12: C1–C4 in Fig. 13).

approximation underestimates the result. This will be discussed in §4.

Figs. 21 – 23 show the ratios: decoupled / eigenvalue result for the PV damage responses at all their positions for the Watt fission spectrum with parameters: MCNP default, neutron-induced fission in ^{235}U and in ^{239}Pu respectively. As expected after taking into account the noise, these results look very similar to those in Figs. 22 – 24 in (Console Camprini et al., 2022) where all the assemblies had the same average axial distribution. In Figs. 21 – 23 the decoupled results at the six positions below the core seem to be smaller overestimates compared with the results at positions A1–A4. (In the case of $\Phi_n > 1$ MeV some results may be underestimated.) This is discussed further in §4.3.

3.2.2. Pin-wise fission source results

3.2.2.1. Pin-wise description. Figs. 24 – 26 show the ratios: decoupled / eigenvalue result for the PV damage responses for the Watt fission spectrum with parameters: MCNP default, neutron-induced fission in ^{235}U and in ^{239}Pu respectively.

In Figs. 24 – 26 we see a substantial improvement over the assembly-wise approximation in Figs. 21 – 23 for all the positions. We also note that as for the pin-wise approximation for the PWR GEN II example, the ^{235}U results are below 1 and the ^{239}Pu results are above 1, and therefore look consistent with the eigenvalue results given the core composition. Instead the default parameter spectrum decoupled results are poorer than the ^{235}U results.

3.2.2.2. Dual pin-wise description. Figs. 27 – 29 show the ratios: decoupled / eigenvalue result at the core mid-plane, at the ex-core detector and in the concrete for the Watt fission spectrum with parameters: MCNP default, neutron-induced fission in ^{235}U and in ^{239}Pu respectively. We see a substantial improvement over the assembly-wise approximation in Figs. 18 – 20, apart from the (n,2n) reaction. We see that now both the PV damage responses at the core mid-plane, the ex-core response and the concrete (n,γ) responses look consistent with the eigenvalue results.

Figs. 30 – 32 show the ratios: decoupled / eigenvalue result for the PV damage responses at all their positions for the Watt fission spectrum with parameters: MCNP default, neutron-induced fission in ^{235}U and in ^{239}Pu respectively. We see in Figs. 31 and 32 that whilst the positions at the core mid-plane look consistent with the eigenvalue results, the positions below the core do not, as most of the ^{235}U spectrum results do, overestimate the decoupled response. Thus if we compare Figs. 30 – 32 with Figs. 24 – 26 containing the single pin results, we see that at the core mid-plane both sets of results seem good. However below the core

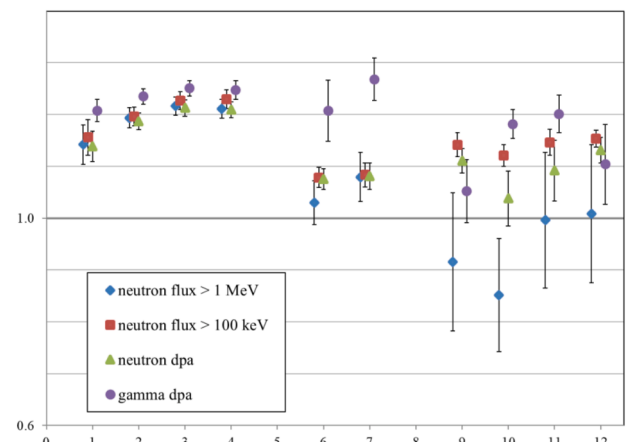


Fig. 22. PWR GEN III: Ratio of decoupled to eigenvalue result for the Watt spectrum for thermal neutron-induced fission in ^{235}U and the assembly-wise description of fission sites (x: 1–4: A1–A4 in Fig. 10; 6, 7: B1, B2 in Fig. 12; 9–12: C1–C4 in Fig. 13).

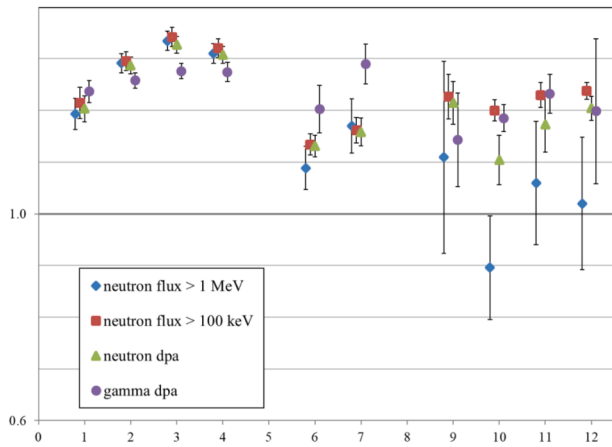


Fig. 23. PWR GEN III: Ratio of decoupled to eigenvalue result for the Watt spectrum for thermal neutron-induced fission in ^{239}Pu and the assembly-wise description of fission sites (x: 1–4: A1–A4 in Fig. 10; 6, 7: B1, B2 in Fig. 12; 9–12: C1–C4 in Fig. 13).

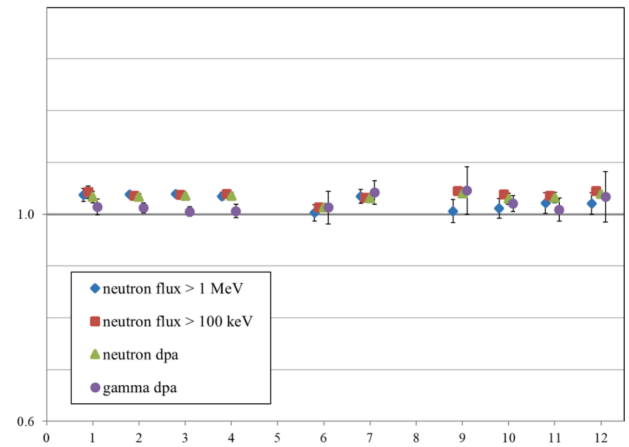


Fig. 26. PWR GEN III: Ratio of decoupled to eigenvalue result for the Watt spectrum for thermal neutron-induced fission in ^{239}Pu and the pin-wise description of fission sites (x: 1–4: A1–A4 in Fig. 10; 6, 7: B1, B2 in Fig. 12; 9–12: C1–C4 in Fig. 13).

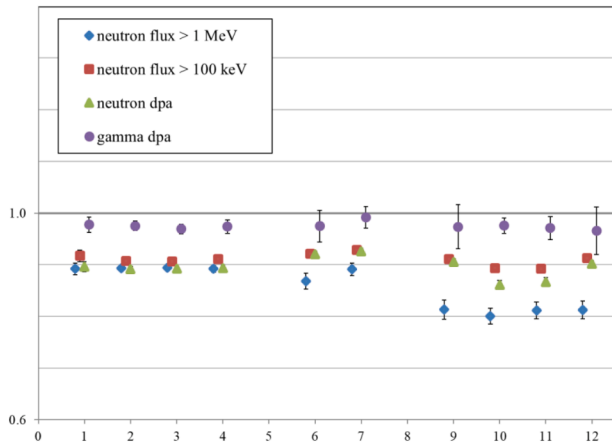


Fig. 24. PWR GEN III: Ratio of decoupled to eigenvalue result for the MCNP default Watt fission spectrum and the pin-wise description of fission sites (x: 1–4: A1–A4 in Fig. 10; 6, 7: B1, B2 in Fig. 12; 9–12: C1–C4 in Fig. 13).

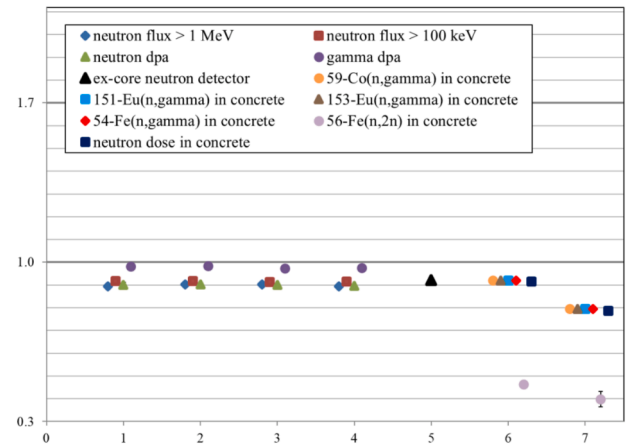


Fig. 27. PWR GEN III: Ratio of decoupled to eigenvalue result for the MCNP default Watt fission spectrum and the dual pin-wise description of fission sites (x: 1–4: A1–A4 in Fig. 10; 5: ex-core detector; 6, 7: concrete shielding at 15, 150 cm depth).

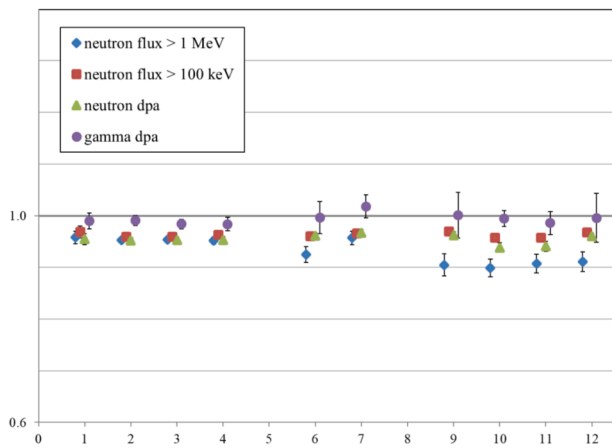


Fig. 25. PWR GEN III: Ratio of decoupled to eigenvalue result for the Watt spectrum for thermal neutron-induced fission in ^{235}U and the pin-wise description of fission sites (x: 1–4: A1–A4 in Fig. 10; 6, 7: B1, B2 in Fig. 12; 9–12: C1–C4 in Fig. 13).

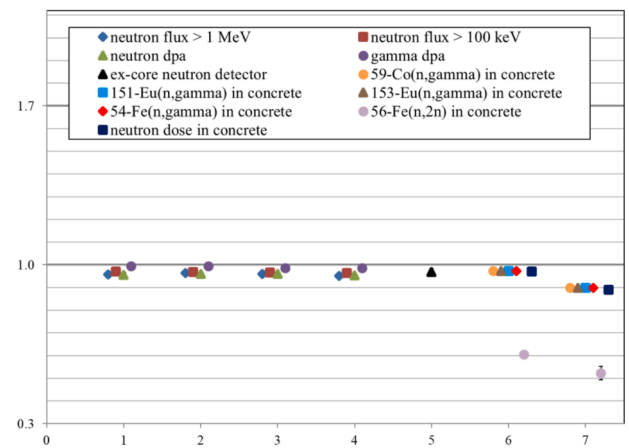


Fig. 28. PWR GEN III: Ratio of decoupled to eigenvalue result for the Watt spectrum for thermal neutron-induced fission in ^{235}U and the dual pin-wise description of fission sites (x: 1–4: A1–A4 in Fig. 10; 5: ex-core detector; 6, 7: concrete shielding at 15, 150 cm depth).

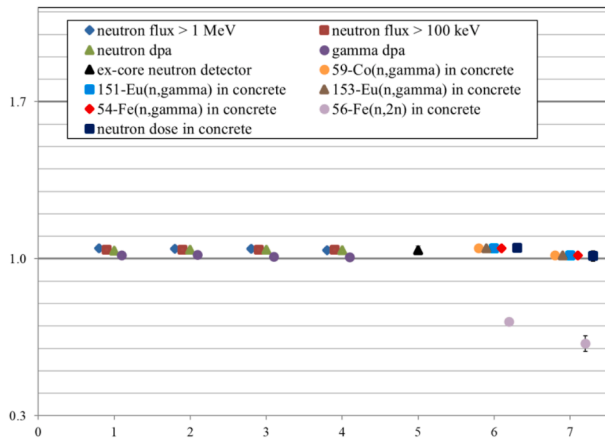


Fig. 29. PWR GEN III: Ratio of decoupled to eigenvalue result for the Watt spectrum for thermal neutron-induced fission in ^{239}Pu and the dual pin-wise description of fission sites (x: 1–4: A1–A4 in Fig. 10; 5: ex-core detector; 6, 7: concrete shielding at 15, 150 cm depth).

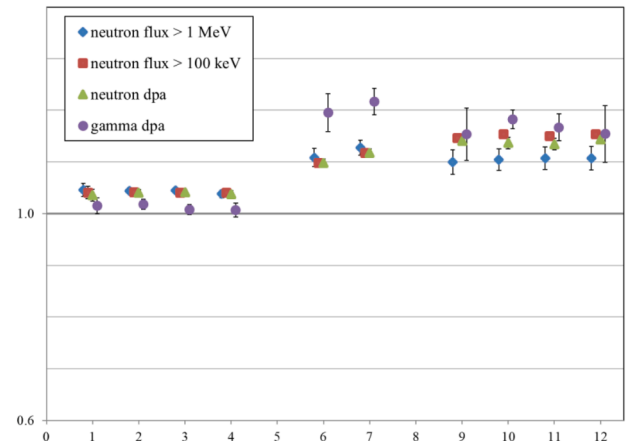


Fig. 32. PWR GEN III: Ratio of decoupled to eigenvalue result for the Watt spectrum for thermal neutron-induced fission in ^{239}Pu and the dual pin-wise description of fission sites (x: 1–4: A1–A4 in Fig. 10; 6, 7: B1, B2 in Fig. 12; 9–12: C1–C4 in Fig. 13).

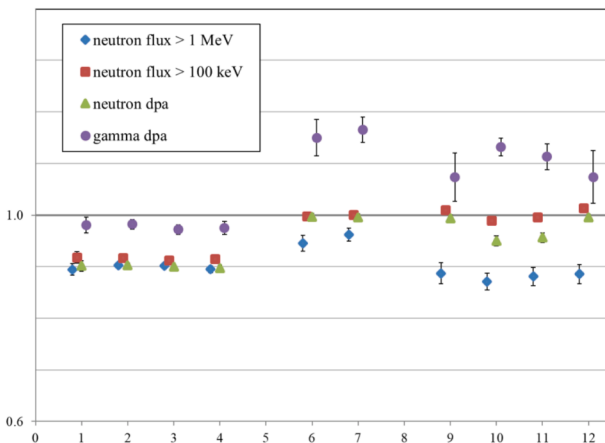


Fig. 30. PWR GEN III: Ratio of decoupled to eigenvalue result for the MCNP default Watt fission spectrum and the dual pin-wise description of fission sites (x: 1–4: A1–A4 in Fig. 10; 6, 7: B1, B2 in Fig. 12; 9–12: C1–C4 in Fig. 13).

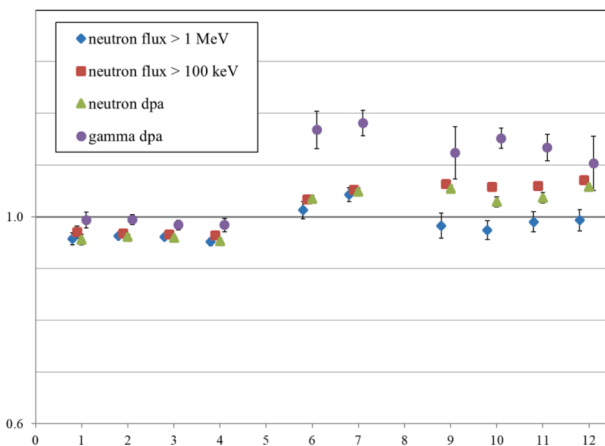


Fig. 31. PWR GEN III: Ratio of decoupled to eigenvalue result for the Watt spectrum for thermal neutron-induced fission in ^{235}U and the dual pin-wise description of fission sites (x: 1–4: A1–A4 in Fig. 10; 6, 7: B1, B2 in Fig. 12; 9–12: C1–C4 in Fig. 13).

the single pin results look better than the dual pin ones. This may be due to error cancellation and is discussed in §4.

3.2.3. Considering the variation of the decoupled response with energy spectrum and with spatial description

We select for this analysis a subset of the responses: positions A3, B2 and C1, (see Figs. 10, 12, 13), the ex-core neutron detectors (see Figs. 14 and 15) and the $^{151}\text{Eu}(n,\gamma)$ rate at both depths in the concrete (Fig. 16). Analogous results at the other positions: A1, A2, A4, B1, C2, C3, C4 and for the other reaction rates: $^{59}\text{Co}(n,\gamma)$, $^{151}\text{Eu}(n,\gamma)$, $^{54}\text{Fe}(n,\gamma)$, $^{56}\text{Fe}(n,2n)$ are given in (Console Camprini et al., 2022).

3.2.3.1. Energy spectrum. We only consider here the dual pin-wise description of the fission sites. Fig. 33-1 – 33-3 show the variation with energy spectrum of the ratios: decoupled / eigenvalue result for the PV damage responses at the positions A3, B2 and C1 respectively. Fig. 33-4 shows the same variation for the ex-core neutron detector and for the $^{151}\text{Eu}(n,\gamma)$ rate at both depths in the concrete.

We see from Fig. 33 that as already noted the decoupled results increase going from the default Watt, through the ^{235}U to the ^{239}Pu spectrum.

In Fig. 33-1 the three neutron responses have a similar gradient. Instead below the core in Fig. 33-2 and 33-3, $\Phi_n > 1$ MeV has a higher gradient compared with $\Phi_n > 100$ keV and dpa_n . In Fig. 33-1 – 33-3 the gamma response is flatter than all three neutron responses. In Fig. 33-4 the variation at 150 cm depth in the concrete is steeper than at 15 cm and for the ex-core detector.

3.2.3.2. Spatial description. Figs. 34 – 36 show the variation with spatial approximation of the ratios: decoupled / eigenvalue result for the PV damage responses at position A3 for the Watt fission spectrum with parameters: MCNP default, neutron-induced fission in ^{235}U and in ^{239}Pu respectively. Figs. 37 – 39 are the same for position B2 and Figs. 40 – 42 are the same for position C1. Finally in Figs. 43 – 45 are shown the variation with spatial approximation of the ratios: decoupled / eigenvalue result for the ex-core detector response and the $^{151}\text{Eu}(n,\gamma)$ reaction rate at 15 and 150 cm depth in the radial concrete.

We see in Figs. 34 – 42 that there is no discernible difference between the mono-axial assembly-wise and the assembly-wise descriptions.

In Figs. 34 – 36 we see that for PV damage responses at the core mid-plane, the two assembly-wise models are situated about $\frac{1}{2}$ way between the homogeneous model and the two pin-wise models. Instead Figs. 43 – 45 indicate that outside the PV in the concrete at the level of the core, the assembly-wise approximation is nearer to the dual pin-wise

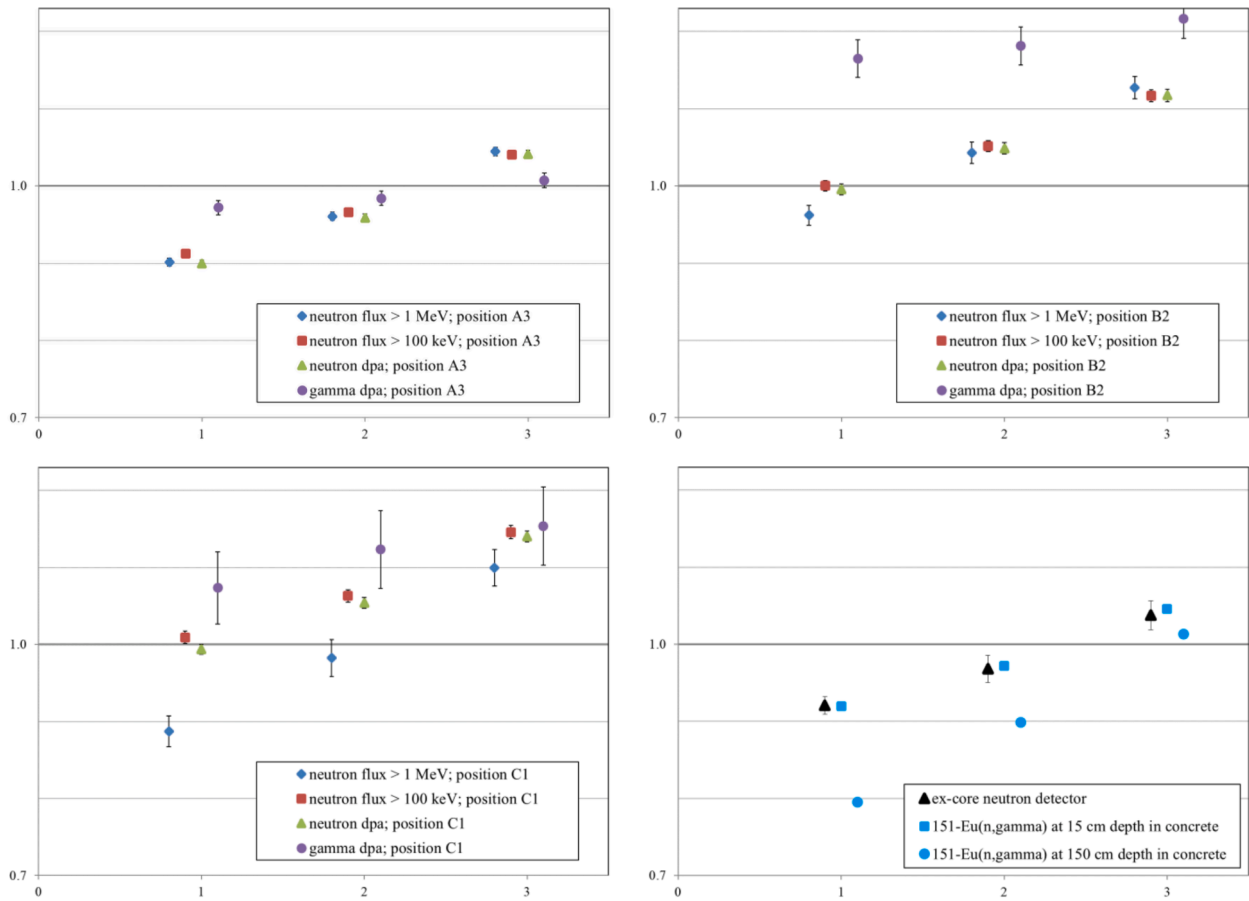


Fig. 33. 1, 33-2, 33-3 and 33-4. PWR GEN III: Ratio of decoupled to eigenvalue result for the dual pin-wise description of fission sites, at positions A3, B2, C1, the ex-core detector and the $^{151}\text{Eu}(n,\gamma)$ rate at 15 cm and 150 cm depths in the concrete, for Watt fission spectra with various parameters (x: 1: MCNP default; 2: thermal neutron-induced in ^{235}U ; 3: thermal neutron-induced in ^{239}Pu).

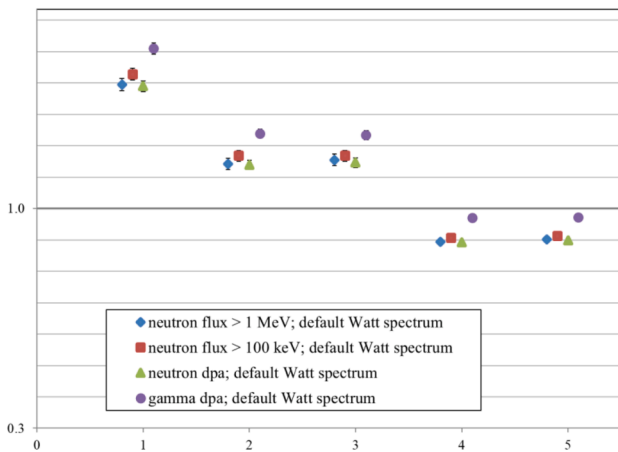


Fig. 34. PWR GEN III: Ratio of decoupled to eigenvalue result at position A3 for the MCNP default Watt fission spectrum and following spatial binning of the fission sites (x: 1: homogeneous; 2: mono-axial assembly-wise; 3: assembly-wise; 4: pin-wise; 5: dual pin-wise).

approximation and farther from the homogeneous model. In Figs. 34 – 36 and 43 – 45 (i.e. at the level of the core) the two pin-wise models look excellent.

Instead for the PV damage responses below the core, Figs. 37 – 42 indicate that the situation is less clear-cut. At positions B2 and C1 the two pin-wise descriptions look only slightly better than the two

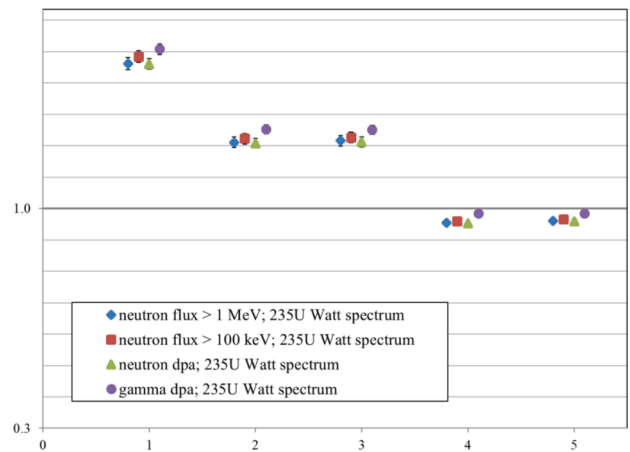


Fig. 35. PWR GEN III: Ratio of decoupled to eigenvalue result at position A3 for the Watt spectrum for thermal neutron-induced fission in ^{235}U and following spatial binning of the fission sites (x: 1: homogeneous; 2: mono-axial assembly-wise; 3: assembly-wise; 4: pin-wise; 5: dual pin-wise).

assembly-wise ones. We deduce that the axial averaging plays an important role for responses below the core compared with those at the level of the core. Also the pin-wise description seems better than the dual pin-wise one.

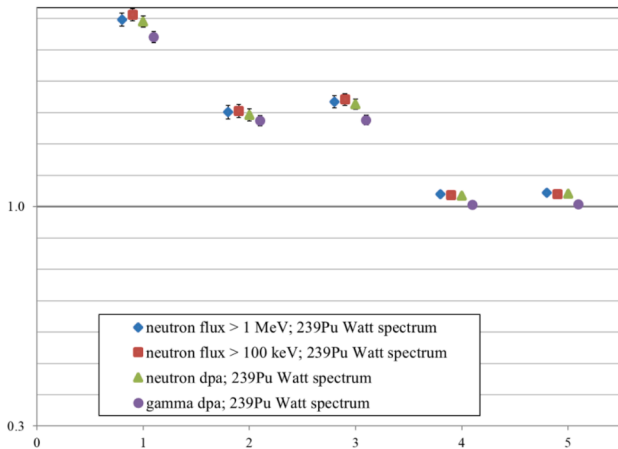


Fig. 36. PWR GEN III: Ratio of decoupled to eigenvalue result at position A3 for the Watt spectrum for thermal neutron-induced fission in ^{239}Pu and following spatial binning of the fission sites (x: 1: homogeneous; 2: mono-axial assembly-wise; 3: assembly-wise; 4: pin-wise; 5: dual pin-wise).

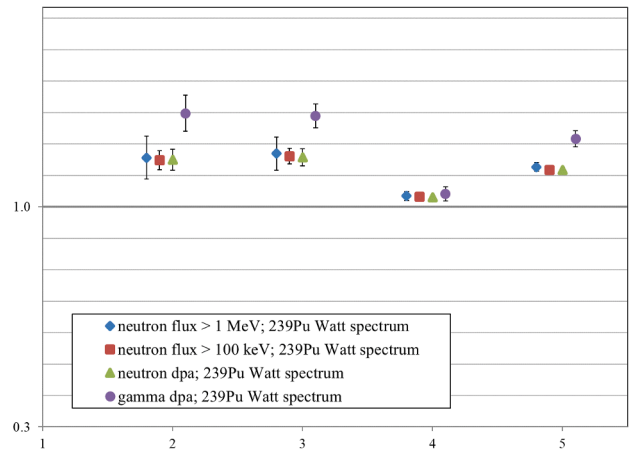


Fig. 39. PWR GEN III: Ratio of decoupled to eigenvalue result at position B2 for the Watt spectrum for thermal neutron-induced fission in ^{239}Pu and following spatial binning of the fission sites (x: 2: mono-axial assembly-wise; 3: assembly-wise; 4: pin-wise; 5: dual pin-wise).

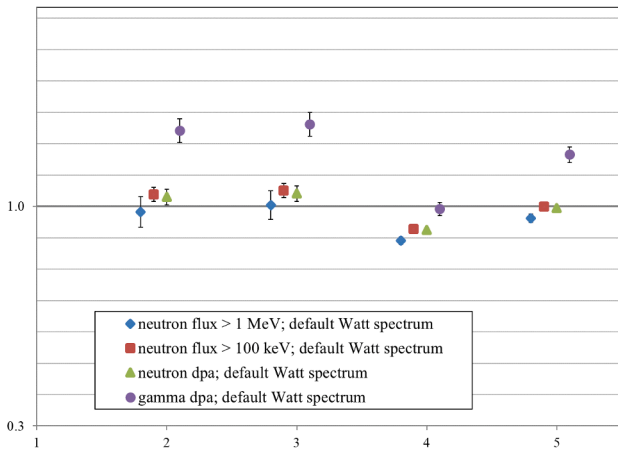


Fig. 37. PWR GEN III: Ratio of decoupled to eigenvalue result at position B2 for the MCNP default Watt fission spectrum and following spatial binning of the fission sites (x: 2: mono-axial assembly-wise; 3: assembly-wise; 4: pin-wise; 5: dual pin-wise).

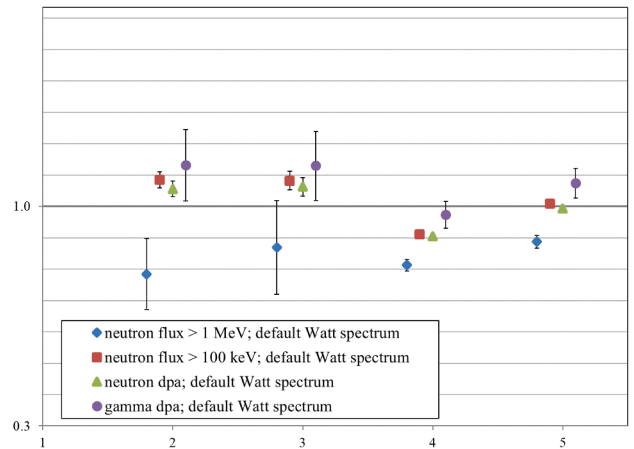


Fig. 40. PWR GEN III: Ratio of decoupled to eigenvalue result at position C1 for the MCNP default Watt fission spectrum and following spatial binning of the fission sites (x: 2: mono-axial assembly-wise; 3: assembly-wise; 4: pin-wise; 5: dual pin-wise).

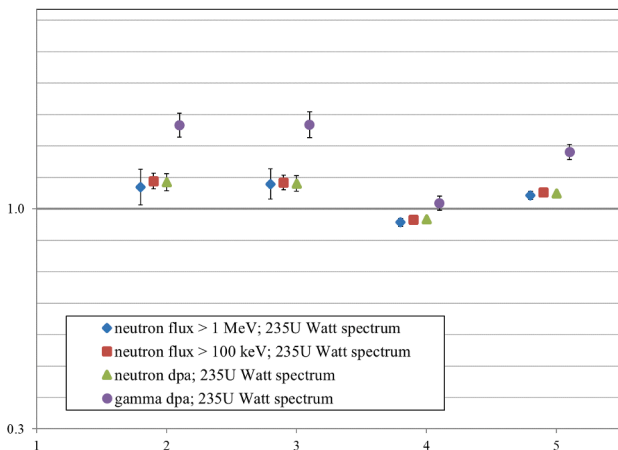


Fig. 38. PWR GEN III: Ratio of decoupled to eigenvalue result at position B2 for the Watt spectrum for thermal neutron-induced fission in ^{235}U and following spatial binning of the fission sites (x: 2: mono-axial assembly-wise; 3: assembly-wise; 4: pin-wise; 5: dual pin-wise).

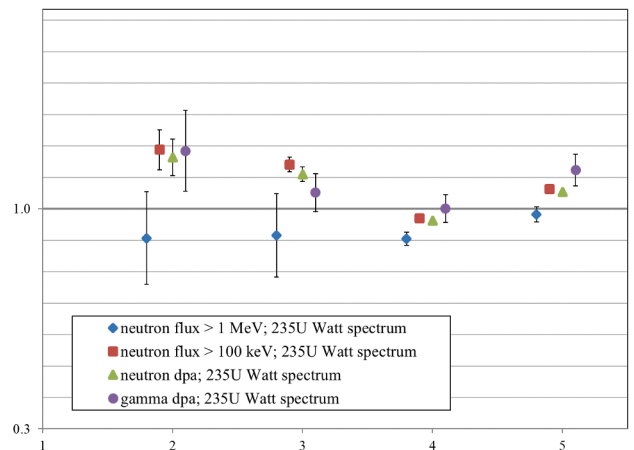


Fig. 41. PWR GEN III: Ratio of decoupled to eigenvalue result at position C1 for the Watt spectrum for thermal neutron-induced fission in ^{235}U and following spatial binning of the fission sites (x: 2: mono-axial assembly-wise; 3: assembly-wise; 4: pin-wise; 5: dual pin-wise).

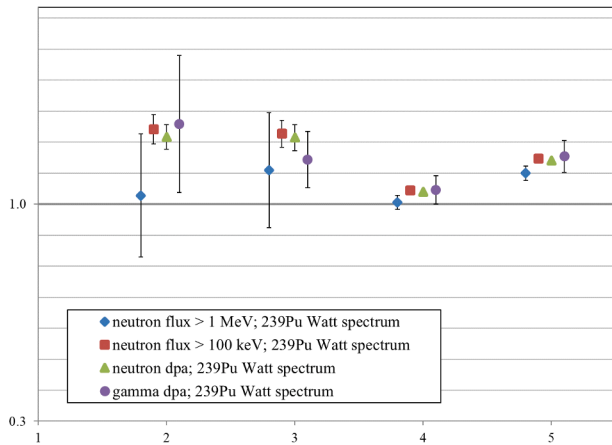


Fig. 42. PWR GEN III: Ratio of decoupled to eigenvalue result at position C1 for the Watt spectrum for thermal neutron-induced fission in ^{239}Pu and following spatial binning of the fission sites (x: 2: mono-axial assembly-wise; 3: assembly-wise; 4: pin-wise; 5: dual pin-wise).

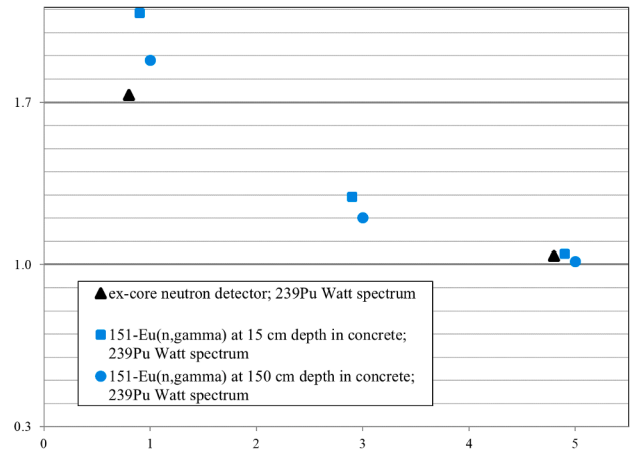


Fig. 45. PWR GEN III: Ratio of decoupled to eigenvalue result for the ex-core detector response and the $^{151}\text{Eu}(n,\gamma)$ rates in the concrete for the Watt spectrum for thermal neutron-induced fission in ^{239}Pu and following spatial binning of the fission sites (x: 1: homogeneous; 3: assembly-wise; 5: dual pin-wise).

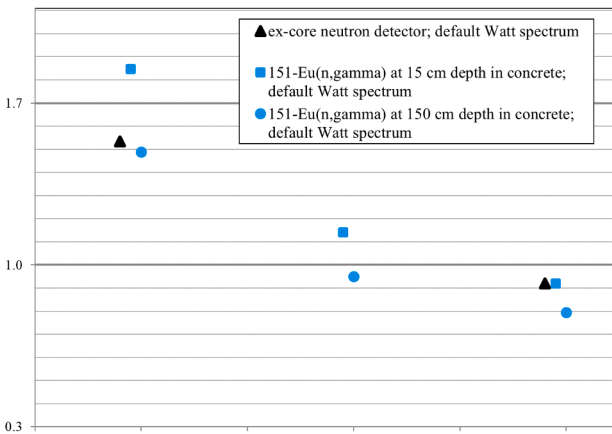


Fig. 43. PWR GEN III: Ratio of decoupled to eigenvalue result for the ex-core detector response and the $^{151}\text{Eu}(n,\gamma)$ rates in the concrete for the MCNP default Watt fission spectrum and following spatial binning of the fission sites (x: 1: homogeneous; 3: assembly-wise; 5: dual pin-wise).

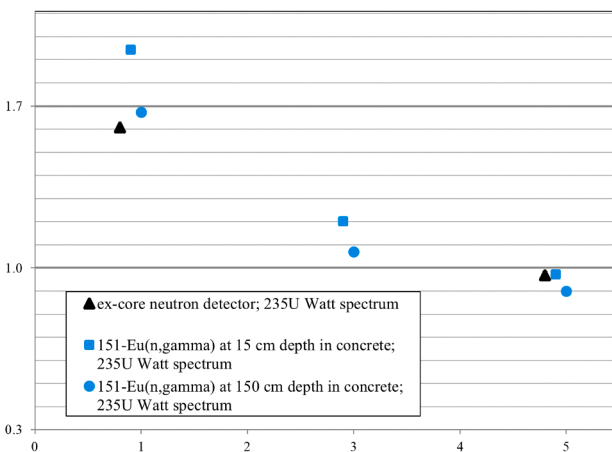


Fig. 44. PWR GEN III: Ratio of decoupled to eigenvalue result for the ex-core detector response and the $^{151}\text{Eu}(n,\gamma)$ rates in the concrete for the Watt spectrum for thermal neutron-induced fission in ^{235}U and following spatial binning of the fission sites (x: 1: homogeneous; 3: assembly-wise; 5: dual pin-wise).

4. Sources of error in the decoupled calculations

At this point it is worth considering the errors in the decoupled approach that derive from the decoupling. They can conveniently be divided into energy and spatial errors:

4.1. Energy

For both reactor models, end-of-cycle fuel compositions were employed. Therefore we would expect the single eigenvalue approach results to lie somewhere between the Watt ^{235}U and ^{239}Pu spectra. Furthermore we assumed *a priori* that the MCNP default Watt spectrum would be a mixture of the ^{235}U and ^{239}Pu spectra.

The latter assumption was wrong – the results with the default Watt spectrum are never between the results of the ^{235}U and ^{239}Pu spectra, but seem instead to come from a softer spectrum – see Fig. 33.

As far as the former assumption is concerned, when one of the two pin-wise spatial models was employed and the responses were at the core mid-plane, with few exceptions the single eigenvalue approach results do indeed tend to lie somewhere between the Watt ^{235}U and ^{239}Pu spectra – see Figs. 7, 8, 25, 26, 28, 29, 33-1, 33-4, 35 (x = 4,5), 36 (x = 4,5), 44 (x = 5) and 45 (x = 5). (Points x = 1 → 4 in Figs. 28 and 29 are seen more clearly in Figs. 31 and 32 due to the larger scale.)

Exceptions to the above are detectors located far from the core which have a higher sensitivity to the fission energy spectrum. In particular the high energy tail of the fission spectra of higher actinides may play a role. Thus in Figs. 18 – 20 and 27 – 29 we have lower results for the responses at 150 cm depth in the concrete compared with 15 cm depth. Also in the same figures both the ^{235}U and ^{239}Pu spectra seriously underestimate the $^{56}\text{Fe}(n,2n)$ rate in the concrete – the threshold of 11.5 MeV means that the high energy tail of the fission distribution becomes very important.

4.2. Space

We list the various averaging approximations that are employed in the decoupled approach:

- Radial averaging over each assembly (“mono-axial assembly-wise description” and “assembly-wise description”): given that the outer assemblies are the predominant contributors ex-core, Figs. 18 – 20 indicate that, notwithstanding the steel reflector in the PWR GEN III model, this averaging overestimates the results.
- Radial averaging over each pin: this averaging underestimates the results. As the two approximations (“pin-wise description” and “dual

pin-wise description”) at positions A1 – A4 in the PWR GEN III model look very similar (compare points $x = 1 \rightarrow 4$ in Figs. 24 and 30, 25 and 31, 26 and 32, also see Figs. 34 – 36), at least for points along the mid-plane, the “pin-wise description” looks sufficient. This may not be the case for responses below the core (see §4.3).

- Axial averaging over each of the 52 bins in the PWR GEN III model may affect the responses below the core. Such averaging will overestimate these responses, especially if there is a contributing channel through the lower plenum. To reduce this overestimate the axial binning was made quite fine at the bottom of the core – see Fig. 17.

4.3. Responses below the core

We observed that for response positions B1, B2 and C1 – C4 in the PWR GEN III model, a non-negligible contributing channel was through the lower plenum (see Figs. 9, 12, 14). This can also be seen from Figs. 21 – 23 where, although the errors are rather large, with the assembly-wise description the responses below the core seem to be smaller overestimates compared with positions A1 – A4. Indeed in some cases they seem to be underestimates.

The existence of a contributing channel through the lower plenum becomes especially important if we have the pin-wise or dual pin-wise radial description. As the neutrons must leak downwards, we can see that the radial variation near the surface of each pin is crucial and the underestimate in §4.2 may be more important than for the case of radial leakage at the level of the core.

Thus taking into account transport through the lower plenum, with the pin-wise description (single or dual) we have a radial averaging giving an underestimate and an axial averaging producing an overestimate. In Figs. 25 and 26 for the pin-wise description the net result looks to be a very slight underestimate for the neutron responses at positions B1, B2 and C1 – C4 (points $x = 6 \rightarrow 12$). Instead in Figs. 31 and 32 for the dual pin-wise description the net result looks to be a small overestimate for the neutron responses and a larger overestimate of the γ responses at these positions, which we see also in Fig. 33-2 and 33-3. We also see these effects in Figs. 38, 39, 41 and 42. Thus for some responses below the core, due to cancellation of errors, the pin-wise description gives slightly better results than the dual pin-wise description.

5. Concluding remarks

We have tested a number of decoupled approximations against a single consistent eigenvalue calculation for some neutronic and gamma responses outside the cores of a PWR GEN II and a PWR GEN III model, both with end-of-cycle fuel compositions.

The responses for the PWR GEN II model were limited to at, or near, the core mid-plane and consisted of the neutron fluxes >1 MeV and >100 keV at 14 azimuthal positions on the inner surface of the PV and the signal from an ex-core neutron detector placed in the PV well. The spatial part of the decoupling involved a pin-wise description with each pin divided into two radial segments. An assembly-wise description was also employed for the ex-core detector.

The responses for the PWR GEN III model consisted again of the neutron fluxes >1 MeV and >100 keV, then in addition neutron and gamma dpa rates on the PV, at four positions at the core mid-plane and six positions below the core. An ex-core neutron detector signal was also considered. Furthermore some typical activation rates were computed at two depths in the radial concrete shielding. The spatial part of the decoupling involved two pin-wise descriptions and two assembly-wise descriptions.

For both the GEN II and III models a homogeneous description of the fission sites within the external surfaces of the core was also run (most of the homogeneous results are reported separately in (Console Camprini et al., 2022)).

The energy at the point of decoupling was treated for both PWR models with three analytic functions based on the Watt fission spectrum.

The GEN II decoupled results with the better pin-wise description lay roughly between 85 and 110 % of the eigenvalue results with the assembly-wise result 20–25 % higher than the pin-wise result for the ex-core signal. The variation with energy spectrum was as expected, apart from the spectrum with default parameters.

The GEN III decoupled results at or around the core mid-plane behaved in a plausible fashion, from the point of view of both the spatial description of the fission sites as well as the modelling of the energy spectrum (again apart from the spectrum with default parameters). The (single) pin-wise spatial description of the fission sites gave acceptable PV damage results at the core mid-plane and radially subdividing each pin did not improve them.

The PV damage responses in GEN III below the core were more difficult to interpret than those at the core mid-plane. Below the core the assembly-wise description was nearly as good as the pin-wise one and the single pin-wise description seemed slightly better than the dual pin-wise one. Transport through the lower plenum meant that averaging over the axial bins seemed to play an important role and the slight superiority of the single pin-wise description over the dual pin-wise one may be due to error cancellation.

CRediT authorship contribution statement

M. Brovchenko: Conceptualization, Methodology, Resources, Writing – original draft, Writing – review & editing. **K.W. Burn:** Conceptualization, Formal analysis, Methodology, Software, Writing – original draft, Writing – review & editing. **P. Console Camprini:** Conceptualization, Formal analysis, Methodology, Software.

Declaration of Competing Interest

The authors declare that they have no known competing financial interests or personal relationships that could have appeared to influence the work reported in this paper.

Data availability

The authors do not have permission to share data.

Acknowledgments

The computing resources and the related technical support used for this work have been provided by CRESO/ENEAGRID High Performance Computing infrastructure and its staff. CRESO/ENEAGRID High Performance Computing infrastructure is funded by ENEA, the Italian National Agency for New Technologies, Energy and Sustainable Economic Development and by Italian and European research programmes, see <http://www.cresco.enea.it/english> for information.

Appendix A. Supplementary data

Supplementary data to this article can be found online at <https://doi.org/10.1016/j.anucene.2022.109417>.

References

- E.D. Blakeman, Neutron and Gamma Fluxes and dpa Rates for HFIR Vessel Beltline Region (Present and Upgrade Designs), ORNL/TM-13693 (2000).
- Brissenden, R.J., Garlick, A.R., 1986. Biases in the estimation of Keff and its error by Monte Carlo Methods. *Ann. Nucl. Energy* 13 (2), 63–83.
- Brovchenko, M., Burn, K.W., Console Camprini, P., 2022. On integrating Monte Carlo calculations in and around near-critical configurations – I. Methodology. *Ann. Nucl. Energy* 172, 109063.
- Burn, K.W., 2014. Optimizing variance reduction in Monte Carlo eigenvalue calculations that employ the source iteration approach. *Ann. Nucl. Energy* 73, 218–240.
- Burn, K.W., 2015. A correction and a clarification to ‘Optimizing variance reduction in Monte Carlo eigenvalue calculations that employ the source iteration approach’. *Ann. Nucl. Energy* 85, 776–777.

- Burn, K.W., Console Camprini, P., A Consistent Monte Carlo Treatment of Radiation Responses in and around Critical Configurations, *Proc. PHYSOR-2018*, Cancun, April 22 – 26, 2018 (track 3, paper 66) pp. 576–586 (2018).
- Burn, K.W., Console Camprini, P., 2017. Radiation transport out from the reactor core: to decouple or not to decouple. *EPJ Web Conf.* **153**, 05007.
- Burn, K.W., Estimating Local In- and Ex-Core Responses within Monte Carlo Source Iteration Eigenvalue Calculations, *Proc. PHYSOR-2014*, Kyoto, Sept. 28 – Oct. 3, 2014, JAEA-Conf 2014-003 paper no. 1228305 (2014a).
- Conlin, J.L., Parsons, D.K., 2014. Release of Continuous Representation for S(α , β) ACE Data, LA-UR-14-21878.
- Conlin, J.L. et al., 2013. Continuous Energy Neutron Cross Section Data Tables Based upon ENDF/B-VII.1, LA-UR-13-20137.
- Console Camprini, P., Burn, K.W., Brovchenko, M., 2021. Monte Carlo with Variance Reduction in and around Near-Critical Configurations, ENEA NK-N-R-570.
- Console Camprini, P., Burn, K.W., Brovchenko, M., 2022. Comparison of Integrated and Decoupled Monte Carlo Results outside Pressurized Water Reactor Cores, ENEA NK-N-R-579 rev.1.
- Goorley, J.T. et al., 2013. Initial MCNP6 Release Overview – MCNP6 version 1.0”, LA-UR-13-22934 Rev.1.
- Konobeyev, A., Voukelatou, K., Displacement Cross-Sections for Materials Irradiated with Neutrons and Protons at the Energies up to 1 GeV, ENEA FIS-P894-012 (2005).
- Sargeni, A., Burn, K.W., Bruna, G.B., 2014. Coupling Effects in Large PWR Reactor Cores: the Impact of Heavy and Conventional Reflectors on Power Distribution Perturbations, *Proc. PHYSOR-2014*, Kyoto, Sept. 28 - Oct. 3, JAEA-Conf 2014-003 paper no. 1099602.
- Trellue, H., Little, R., 2008. Release of New MCNP S(α , β) Library ENDF70SAB Based on ENDF/B-VII.0, LA-UR-08-3628.
- Veinot, K.G., Hertel, N.E., 2005. Effective quality factors for neutrons based on the revised ICRP/ICRU recommendations, *Radiat. Prot. Dosim.* **115** 1-4 536.
- Vuiart, R., Console Camprini, P., Burn, K.W., Brovchenko, M., Taforeau, J., Dumonteil, E., 2021. Impact of Fission Spectrum Modeling on Aging Estimations of Pressurized Water Reactor Vessels, *Trans. Am. Nucl. Soc. Winter Meeting*, Washington DC, Nov. 30 – Dec. 3, 2021, in *Computational Methods for Radiation Protection and Shielding*, pp. 1106-1109.